The Oxidation Behavior of UO_2 in air at 573–723 K

Hyounggyu Park, Kwangheon Park*
Department of Nuclear Engineering, Kyunghee University, Kyunggi-do, 446-701, Korea
**Corresponding author: kpark@khu.ac.kr*

1. Introduction

It is necessary to study the phenomena of UO_2 oxidation in air. During the dry storage period, there is a possibility that the pellet inside the cladding can be oxidized, if the cladding has pinholes or small cracks. The formation of U_3O_8 leads to an approximately 23% density decrease and a 36% volume increase. Thus, the volume expansion causes fuel fracture and small cracks larger at cladding, which release radioisotope outside [1].

Two oxidation mechanisms are recognized for un-irradiated UO_2, from UO_2 to U_3O_7, and from U_3O_7 to U_3O_8 [2]. Oxidation from UO_2 to U_3O_8 occurs over two steps at powder. After U_3O_7 is transformed from UO_2, U_3O_8 is formed from the U_3O_7. Unlike for UO_2 powder, it has been identified that U_3O_8 exists at the early stage of the UO_2 oxidation at fragment [3].

Experiments on the oxidation kinetics of UO_2 fragments were performed at temperatures of 573, 623, 673, and 723 K. And in order to see the existence of U_3O_8 at the early stage, XRD was used with the sample by the time step oxidation at 573 K.

The main objectives of this work is to compare and to analyze the phenomena of UO_2 oxidation between powder and fragment. Also a relative surface-to-volume model is proposed to explain the phenomena of UO_2 fragment oxidation at 573 - 723 K.

2. Materials and method

2.1. Sample preparation from UO_2 pellet

The average flow-ability of UO_2 pellets is 1.47 g/cc and the average density is 10.73 g/cm^3 (97.9% of theoretical density). The mean grain size is 14.7 µm. The UO_2 pellets were cut into disk shaped samples. The average radius and the height of the samples was 3.6 mm and 2 mm, respectively. The samples were then broken into large and small fragments in Fig. 1.

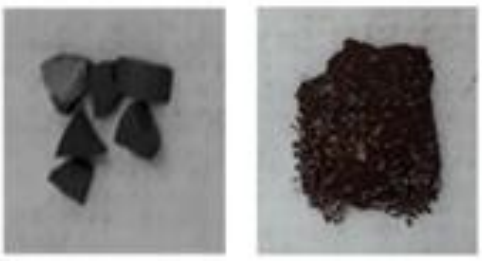

Fig. 1. Large (left) and small (right) fragments from the disk-type samples.

2.2. Procedure

The experiments were conducted using a thermogravimetric analyzer (SETARAM, TGA 92-12) at atmospheric pressure in air. The experiments were carried out at 573, 623, 673, and 723K. The flow rate of air was 10 L/h and the ramping temperatures were 30, 35, 40, and 45 °C/min, respectively. The stoichiometry was determined based on the weight increase. The experiments were continued until the weight gain, and thus stoichiometry, was constant.

The experiment of UO_2 fragment oxidation in muffle furnace was conducted at 573 K for 9 hours to figure out the existence of U_3O_8 at the early stage. After taking out the samples, the weight change of the samples was checked with the electronic balance. And the phases of the UO_2 sample was also analyzed with the XRD measurement (D2 PHASER, BRUKER).

3. Results and Discussion

3.1. Comparison between powder and fragment

Fig. 2 shows the TG curves of UO_2 powder and a fragment at the constant temperature, 623 K, in air. Two types of oxidation were observed at powder while one type of oxidation was shown at the fragment. In the powder case, U_3O_7 was detected at the first plateau and U_3O_8 was observed at the second plateau without U_3O_7. However, a plateau was observed in the case of fragment. It is expected that U_3O_8 would exist at the early stage of TG curve [3].

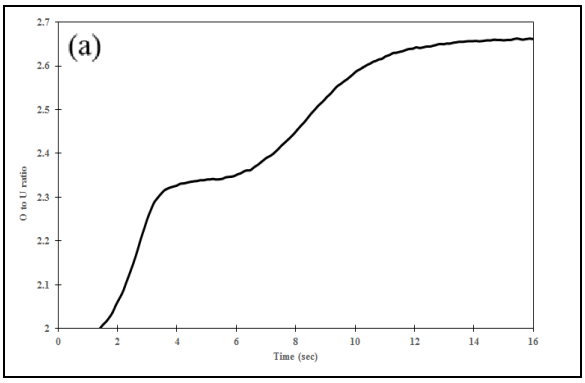

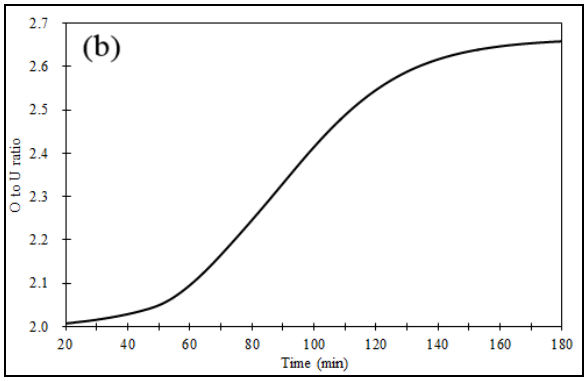

Fig. 2. Reaction curve of the transition from UO_2 to U_3O_8, (a) powder and (b) fragment at 623 K.

Fig. 3 shows the phase change of $UO_{2.13}$ fragment, it was identified as $UO_{2.13}$ after measuring with XRD, in air at 573 K with increasing time. After 6.5 h, the weight increased around 0.3% and small intensities of U_3O_7 was observed instead of U_3O_8. After 9 h, the weight increased about 0.5 % and the intensities of U_3O_8 was observed. In the case of powder, after the percentage of weight gain was over 1.98%, U_3O_8 was observed. In contrast, even though the percentage of weight gain at fragment was 0.5 %, U_3O_8 was detected.

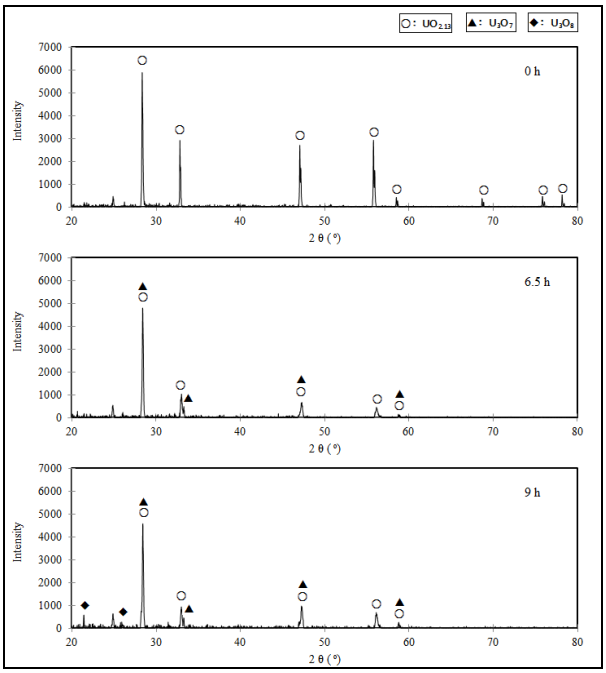

Fig. 3. Change of XRD patterns for the products of $UO_{2.13}$ fragment heated at 573 K in air with increasing time.

Fig. 4 indicates the schematic illustration to explain the different process of formation of U_3O_8 between powder and fragment. After U_3O_7 is transformed from UO_2, U_3O_8 is formed from U_3O_7. Unlike for UO_2 powder, U_3O_8 is formed from U_3O_7 at the fragment even if there is UO_2 inside the fragment. It is considered that time for forming U_3O_8 from U_3O_7, nucleation and growth, is faster than oxygen diffusion for transition from UO_2 to U_3O_7. Fig. 2 and Fig. 3 are the evidence of the concept of Fig. 4.

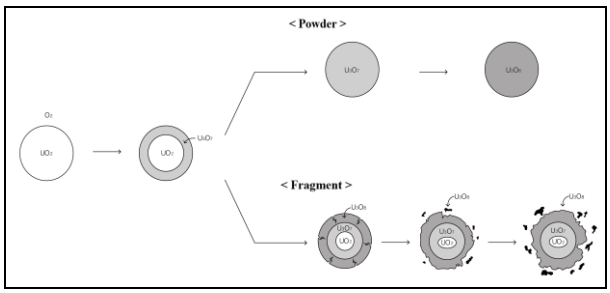

Fig. 4. Schematic image of UO_2 oxidation at powder and fragment.

3.2. New model of phenomenology at fragment

A new model of the relative surface-to-volume focuses on the volume expansion and the change in surface area according to oxidation time. The concept of volume expansion and change in surface area is based on the geometric physical model, referred from bacterial cell size model [4]. Some assumptions are inherent in the relative surface-to-volume model.

- The fraction of transition from UO_2 is proportional to the stoichiometry of UO_{2+x}.
- Volume and surface are time-dependent functions.
- The volume increases exponentially.
- Increased volume affects the change of surface.
- Cracking occurs constantly with time.

$$x(t) = x_{eq} + \left(x_0 - x_{eq}\right) \cdot e^{-\int_0^t f(t)dt} . \quad (1)$$

Eq. (1) is the phenomenological model [5]. The factors influencing the oxidation rate are denoted as $f(t)$, which is $(K_{phen} \cdot S(t))/(\rho_u \cdot V(t))$. $S(t)/V(t)$ is the surface-to-volume ratio, and K_{phen} and ρ_u are the rate constant and molar density of uranium in UO_2 respectively. And x_0 is the initial stoichiometry of UO_2 and x_{eq} is the equilibrium stoichiometry of U_3O_8. Also t is the time required for oxidation and can be determined experimentally.

$$\frac{dV(t)}{dt} = \alpha \cdot \left(V(t) - c\right). \quad (2)$$

It is assumed that the volume increases exponentially with time. The deviation of the volume, $V(t)$, at time t is influenced by conversion factor, c, which is used to deal

with the effect of cracking, and α is a volume growth rate constant.

$$\frac{dS(t)}{dt} = \beta \cdot \left(V(t) - c\right). \quad (3)$$

The surface could be affected by the volume change because the volume expansion and cracking make the surface more reactive. Namely, the surface area could increase with the increased volume. In Eq. (3), β is a constant linking the surface growth rate constant to the current volume.

After solving for $f(t)$ with Eq. (2) and Eq.(3), some values are substituted with the constants A_1, A_2, and A_3 because the values are considered as constant values. Where A_1 is $(K_{phen} \cdot \beta)/(\rho_u \cdot \alpha)$, A_2 is $(V_0 - c)/c$ and A_3 is $(V_0 - (\alpha/\beta) \cdot S_0)/c$. V_0 and S_0 are the initial volume of the sample and the initial surface area of the sample, respectively

$$x(t) = \frac{8}{3} - \frac{2}{3} \cdot \left(\left(\frac{1 + A_2}{1 + A_2 \cdot e^{\alpha t}} \right)^{\frac{A_1 A_3}{\alpha}} \cdot e^{A_1 \cdot (A_3 - 1) t} \right). \quad (4)$$

Eq. (4) is the new relative surface-to-volume model, focusing on the time-dependent surface-to-volume ratio for $x(t)$. The constants A_1, A_2, A_3, and α are obtained empirically using MATLAB code and tend differ with the temperature and sample size.

3.3. Comparison of experimental data and relative surface-to-volume model.

The values in Table I and Table II were calculated using the least squares and Gauss-Newton methods via MATLAB code. The values of A_1 and α for the small fragments are higher than for the large fragments because the ratio of surface to volume is higher. The values of A_1, A_2, and α at both sizes increase with increasing temperature.

Table I: The values of A_1, A_2, A_3, and α for large fragments at 573, 623, 673, and 723 K

Temp. (K)	A_1	A_2	A_3	α
573	0.86E-4	9.54E-3	0.984	1.27E-4
623	7.33E-4	1.99E-2	1.021	0.77E-3
673	1.37E-3	3.19E-2	0.928	1.83E-3
723	2.82E-3	5.51E-2	0.914	1.20E-3

Table II: The values of A_1, A_2, A_3, and α for small fragments at 573, 623, 673, and 723 K

Temp. (K)	A_1	A_2	A_3	α
573	1.41E-4	9.40E-3	0.985	1.85E-4
623	9.10E-4	1.99E-2	0.973	1.19E-3
673	1.86E-3	3.17E-2	0.849	2.10E-3
723	3.58E-3	5.74E-2	0.932	1.60E-3

Fig. 5 shows comparisons between the experimental data for large and small fragments and the relative surface-to-volume model at each temperature (573, 623, 673, and 723 K). The new model is in agreement with the experimental results. Furthermore, the relative surface-to-volume model explains the influence of cracking with the time-dependent surface-to-volume ratio.

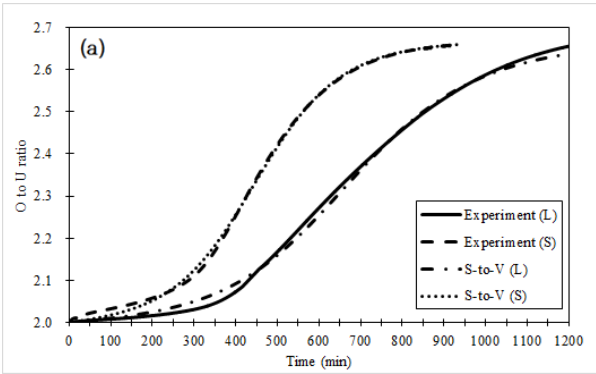

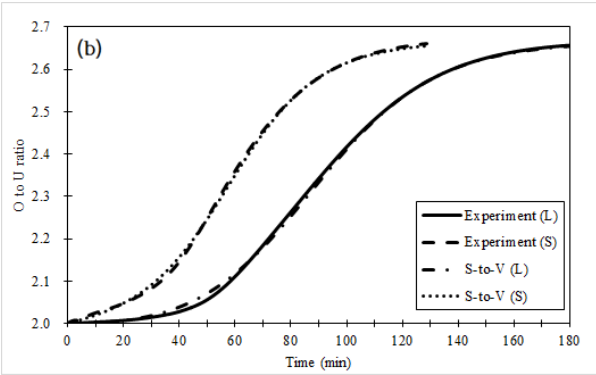

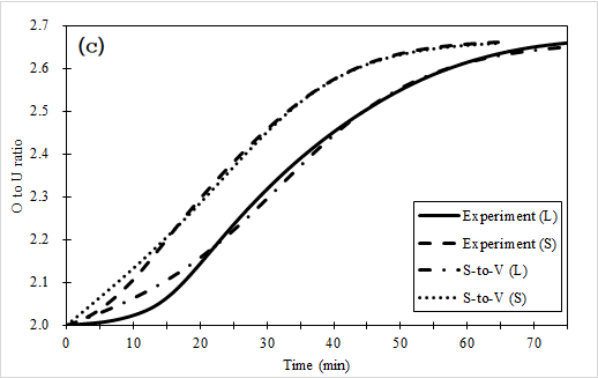

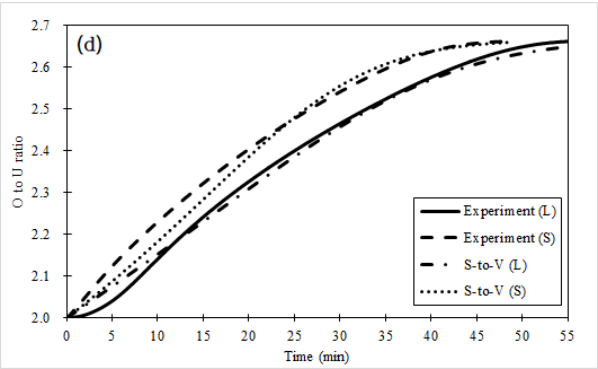

Fig. 5. Comparison of the experimental O to U ratio of large and small fragments with the relative surface-to-volume model at (a) 573 K, (b) 623 K, (c) 673 K, and (d) 723 K.

4. Conclusions

Experiments on the oxidation of UO_2 fragments were conducted at 573, 623, 673, and 723 K. Also experiment of $UO_{2.13}$ fragment in muffle furnace was performed to observe the existence of U_3O_8 at the initial stage.

Powder and fragment have the different process of formation of U_3O_8 on the oxidation. In the case of the powder, U_3O_8 is formed after U_3O_7 is transformed from UO_2. In contrast, the fragment has UO_2, U_3O_7, and U_3O_8 together during oxidation process. To describe the processes, the schematic image was suggested in this research paper.

A new model was proposed to explain the curve, sigmoidal curve, of the oxidation of UO_2 fragments. The surface-to-volume ratio changes with oxidation time due to cracking, leading to increased volume expansion. As a result, the new model applies the effect of cracking based on the surface-to-volume ratio. And the model is in close agreement with the experimental results.

REFERENCES

[1] G. Rousseau, L. Desgranges, F. Charlot, N. Millot, J.C. Ni e`pce, M. Pijolat, F. Valdivieso, G. Baldinozzi, J.F. Be`rar, “A detailed study of UO2 to U3O8 oxidation phases and the associated rate-limiting steps”, Journal of Nuclear Materials, **355**, 10 (2006).

[2] L.E. Thomas, R.E. Einziger, H.C. Buchanan, “Effect of fission products on air-oxidation of LWR spent fuel”, Journal of Nuclear Materials, **201**, 310 (1993).

[3] P. Taylor, D.D. Wood, A.M. Duclos, “The early stages of U_3O_8 formation on unirradiated CANDU UO_2 fuel oxidized in air at 200-300°C”, Journal of Nuclear Materials, **189**, 116 (1992).

[4] L.K. Harris, J.A. Theriot, "Relative rates of surface and volume synthesis set bacterial cell size", Cell, **165,** 1479 (2016).

[5] D.R. Olander, "Mechanistic interpretations of UO2 oxidation", Journal of Nuclear Materials, **252**, 121 (1998).